Current Profile Control for the Development of Consistent Discharges in DIII-D

William Wehner, Justin E. Barton, Mark D. Boyer, Eugenio Schuster, Tim C. Luce, John R. Ferron, Michael L. Walker, David A. Humphreys, Ben G. Penaflor and Robert D. Johnson

***Abstract*— The number of tokamak discharges required to carry out meaningful experiments can be significantly reduced by current profile control in the early startup phase. The tokamak is a plasma-confinement device, suitable for confining plasma at the requisite high temperature necessary for initiating fusion. It is currently the most promising device for realizing sustained fusion power generation at a commercial grade level, though it is still in the experimental stage. Presently, the desired plasma startup conditions, such as the shape of the plasma current profile, are achieved in a trial and error fashion, which can be a lengthy, wasteful process. In this work we make use of model-based control techniques such as optimal feedforward control via nonlinear programming and linearized feedback control to obtain a target current profile at a specified time in low-confinement-mode (L-mode) discharges. The effectiveness of the controller is demonstrated experimentally.**

I. Introduction

Modern tokamak operation requires continuous heat input from auxiliary sources and inductive current drive from external coils. A current ramp-up is required in the inductive coils to drive the plasma current, so present-day tokamaks are naturally limited to short "discharges" due to current limits in the inductive coils. The key to realizing commercially viable fusion energy production is finding a certain operating scenario that will allow for a self driven noninductive plasma current and a long heat confinement time. Such a scenario is often referred to as an advanced tokamak (AT) scenario [1]. It is widely believed that the precursor to realizing the AT scenario involves optimization of the spatial distribution of the current profile [2]. Certain current profile shapes have demonstrated improved confinement, magnetohydrodynamic stability, and a high fraction of self-generated current by the "bootstrap" effect [3], which could potentially enable high gain, steady-state reactor operation.

In order to conduct meaningful experiments, it is necessary to reliably reproduce the desired plasma conditions in repeated discharges. In particular, accurate control of the current profile in the early startup phase is crucial to obtaining reproducibility between discharges. Presently, the current profile is controlled via a purely feedforward trial and error fashion. Typically, some preheating by neutral beam injection (NBI) at DIII-D [4] or lower-hybrid (LH) current drive at other tokamaks such as JT-60U [5] is applied during the start-up phase to modify the relaxation rate of the current profile. Trials are repeated until an adequate timing of the strong NBI heating triggers the desired improvement of the plasma performance. Naturally this process involves a lot of wasted discharges before the primary experiment begins. We propose a combined feedforward+feedback control approach to improve reproducibility between shots and save experimental time.

The dynamic evolution of the current profile is nonlinearly coupled with several plasma parameters including the densities and temperatures of electrons and ions. Thus, an exhaustive modeling of the current profile evolution involves many nonlinear partial differential equations. In this work, we use a first-principles-driven, control-oriented model of the current profile evolution suitable for low confinement (L-mode) discharges in DIII-D. Advances towards developing low-order, "control-oriented" models for current profile control in various tokamaks are discussed in [6], [7], [8], [9]. The models generally combine the magnetic diffusion equation [10] with empirical correlations for the electron temperature, resistivity, and noninductive current drive. Recently, model-based current profile control has undergone rapid development by using various techniques [11], [12], [13], [14].

The motivating objective of this work is to improve reproducibility of discharges with current control in the early startup phase. Specifically, we wish to achieve certain current profile targets during the L-mode phase of the discharge in DIII-D while avoiding transitions into the higher confinement mode (H-mode) [15]. This equates to a critical limit on the auxiliary power input to prevent the L-H transition. Available actuators to manipulate the profile include the NBI and the total plasma current. We elect to not use electron cyclotron current drive (ECCD) since the auxiliary power limit is significantly constrained by the L-H transition threshold and there is simply not enough room for additional ECCD power.

The proposed control method involves both optimal feedforward control via nonlinear programming and optimal state feedback control with integral action to eliminate deviations from the desired trajectory. This work is organized as follows. The model structure and effects of the actuators are described in Section II, details of the feedforward+feedback control design approach are given in Section III, experimental evidence of the effectiveness of the controller in reaching the target is presented in Section IV, and, finally, conclusions are made in Section V.

This work was supported in part by the U.S. Department of Energy (DE-SC0010661, DE-FC02-04ER54698). W. Wehner (wehner@lehigh.edu), J.E. Barton, M.D. Boyer, and E. Schuster are with the Department of Mechanical Engineering and Mechanics, Lehigh University, Bethlehem, PA 18015, USA. M.L. Walker, J.R. Ferron, T.C. Luce, D.A. Humphreys, B.G. Penaflor, and R.D. Johnson are with General Atomics, San Diego, CA 92121, USA.

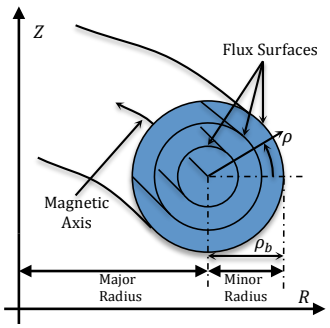

Fig. 1. Magnetic configuration of a tokamak (field lines follow a helical path around the tokamak). Flux surfaces represent points of constant poloidal magnetic flux.

II. Modeling the Current Profile Evolution

Following any magnetic field line a number of times around the torus a closed flux tube is mapped, a so called magnetic-flux surface, which marks points of constant poloidal magnetic flux, Ψ. The values of Ψ on these flux surfaces along the plasma radial coordinate (ρ in Fig. 1) is called the poloidal magnetic flux profile. In order to index the flux surfaces in Fig. 1, this work makes use of the mean effective minor radius, ρ. It can be expressed in terms of the toroidal magnetic flux, Φ, and the toroidal field strength at the plasma center, $B_{\phi,0}$, i.e. $\pi B_{\phi,0}\rho^2 = \Phi$. Normalized ρ, denoted by $\hat{\rho}$, is defined as ρ/ρ_{b}, where ρ_{b} is the value of ρ at the last closed magnetic flux surface. The q profile, a measure of the magnetic twist[1], is related to the spatial gradient of the poloidal magnetic flux, Ψ, and is defined as

$$q(\hat{\rho},t) = \frac{d\Phi}{d\Psi} = -\frac{d\Phi}{2\pi d\psi} = -\frac{B_{\phi,0}\rho_{\mathrm{b}}^2\hat{\rho}}{\partial\psi/\partial\hat{\rho}}, \tag{1}$$

where t is the time and ψ is the poloidal stream function, which is closely related to the poloidal flux, i.e. $\Psi = 2\pi\psi$. As the q profile depends inversely on the spatial derivative of the poloidal flux, we define the terms

$$\theta(\hat{\rho},t) \triangleq \frac{\partial\psi}{\partial\hat{\rho}}(\hat{\rho},t), \quad \iota(\hat{\rho},t) \triangleq \frac{1}{q(\hat{\rho},t)} \triangleq \frac{-\theta}{B_{\phi,0}\rho_{\mathrm{b}}^2\hat{\rho}}, \tag{2}$$

which will be useful for control purposes.

The evolution of the poloidal magnetic flux can be described by the magnetic diffusion equation [10],

$$\frac{\partial\psi}{\partial t} = \frac{\eta(T_{\mathrm{e}})}{\mu_0\rho_{\mathrm{b}}^2\hat{F}^2}\frac{1}{\hat{\rho}}\frac{\partial}{\partial\hat{\rho}}\left(\hat{\rho}\hat{F}\hat{G}\hat{H}\frac{\partial\psi}{\partial\hat{\rho}}\right) + R_0\hat{H}\eta(T_{\mathrm{e}})j_{\mathrm{NI}}, \tag{3}$$

where $\eta(T_{\mathrm{e}})$ is the plasma resistivity for which simplified scaling models are available [16], [17], T_{e} is the electron temperature, μ_0 is the vacuum permeability, j_{NI} is the noninductive current density from various sources, $\hat{F}$, $\hat{G}$, and $\hat{H}$ are spatially varying geometric factors pertaining to the magnetic configuration of a particular plasma equilibrium [6]. The boundary conditions are given by

$$\left.\frac{\partial\psi}{\partial\hat{\rho}}\right|_{\hat{\rho}=0} = 0, \quad \left.\frac{\partial\psi}{\partial\hat{\rho}}\right|_{\hat{\rho}=1} = -\frac{\mu_0}{2\pi}\frac{R_0}{\hat{G}|_{\hat{\rho}=1}\hat{H}|_{\hat{\rho}=1}}I_{\mathrm{p}}(t), \tag{4}$$

[1]The q profile is directly related to the current profile and they are often referred to interchangeably. In the remainder of the work we will refer solely to the q profile.

where $I_{\mathrm{p}}(t)$ is the total plasma current. Based on experimental observations at DIII-D, simplified scenario-oriented empirical models for the plasma density, electron temperature, plasma resistivity and noninductive current density during L-mode discharges were identified [9].

For simplicity, we rewrite the model (3) in a control-oriented form,

$$\begin{aligned}\frac{\partial\psi}{\partial t}(\hat{\rho},t) &= \frac{f_\eta}{\hat{\rho}}\frac{\partial}{\partial\hat{\rho}}\left(\hat{\rho}D_\psi\frac{\partial\psi}{\partial\hat{\rho}}\right)u_\eta(t)\\ &+\sum_{i=1}^{n_{\mathrm{NBI}}} f_{\mathrm{NBI},i}u_{\mathrm{NBI},i}(t) + f_{\mathrm{BS}}\left(\frac{\partial\psi}{\partial\hat{\rho}}\right)^{-1}u_{\mathrm{BS}}(t),\end{aligned} \tag{5}$$

with the boundary conditions,

$$\left.\frac{\partial\psi}{\partial\hat{\rho}}\right|_{\hat{\rho}=0} = 0, \qquad \left.\frac{\partial\psi}{\partial\hat{\rho}}\right|_{\hat{\rho}=1} = k_{I_{\mathrm{p}}}(t)I_{\mathrm{p}}(t). \tag{6}$$

The term n_{NBI} denotes the number of neutral beam injectors, $D_\psi = \hat{F}\hat{G}\hat{H}$, the functions $f_{(\cdot)}(\hat{\rho})$ capture the spatial dependence of the model and $u_{(\cdot)}(t)$ are a set of nonlinear input functions of the form,

$$\begin{aligned}u_\eta(t) &= I_{\mathrm{p}}(t)^{-3/2}P_{\mathrm{tot}}(t)^{-3/4}\bar{n}_{\mathrm{e}}(t)^{3/2},\\ u_{\mathrm{NBI},i}(t) &= I_{\mathrm{p}}(t)^{-1}P_{\mathrm{tot}}(t)^{-1/2}P_{\mathrm{NBI},i}(t),\\ u_{\mathrm{BS}}(t) &= I_{\mathrm{p}}(t)^{-1/2}P_{\mathrm{tot}}(t)^{-1/4}\bar{n}_{\mathrm{e}}(t)^{3/2}.\end{aligned} \tag{7}$$

The form of these functions arise from the empirical correlations for density, temperature, and auxiliary current drive; they admit diffusivity control, u_η, interior control, $u_{\mathrm{NBI},i}$ and u_{BS}, and boundary control, I_{p}. Using (2), we can obtain from (5) an equation for the evolution of θ (see [18] for details), i.e.,

$$\begin{aligned}\frac{\partial\theta}{\partial t} =& h_0u_\eta\theta'' + h_1u_\eta\theta' + h_2u_\eta\theta\\ &+\sum_{i=1}^{n_{\mathrm{NBI}}} f_{\mathrm{NBI},i}u_{\mathrm{NBI},i} + f'_{\mathrm{BS}}\frac{1}{\theta}u_{\mathrm{BS}} - f_{\mathrm{BS}}\frac{1}{\theta^2}u_{\mathrm{BS}},\end{aligned} \tag{8}$$

along with boundary conditions $\theta|_{\hat{\rho}=0} = 0$, $\theta|_{\hat{\rho}=1} = -k_{I_{\mathrm{p}}}I_{\mathrm{p}}$, where $(\cdot)' = \partial/\partial\hat{\rho}$, the time and space dependencies are dropped for simplicity, and the functions, $h_{(\cdot)}$, which were introduced for compactness, can be written in terms of the $f_{(\cdot)}$ functions.

III. Feedforward plus Feedback Control

A. Feedforward Control via Nonlinear Programming

The design of the FF control can be formulated as a nonlinear optimization problem. The details of the problem formulation and optimization procedure are outlined in [19]. In summary, the feedforward control is solved according to

$$\begin{aligned}P = \underset{u_{\mathrm{FF}}}{\text{minimize}} \quad & J(\psi(t_{\mathrm{targ}}),\psi_{\mathrm{targ}})\\ \text{subject to} \quad & \psi\text{-dynamics governed by (3)} - \text{(4)},\\ & \psi(t_0)\ \text{(initial condition)},\\ & g_1(u_{\mathrm{FF}}) \le 0,\ \ g_i(u_{\mathrm{FF}}) \le 0,\end{aligned}$$

where ψ_{targ} represents the target profile, t_{targ} is the desired time of reaching the target profile, $J(\psi(t_{\mathrm{targ}}),\psi_{\mathrm{targ}})$ is a

quadratic cost function which penalizes deviations from the desired target profile, $g_1(u_{\text{FF}})$ is a nonlinear constraint which prevents L-H transition, and $g_i(u_{\text{FF}})$ is a set of linear constraints that account for the actuator limits (subindex i denotes different actuators). The result is a feedforward control policy given by $u_{\text{FF}} = \arg\min P$ and a corresponding reference trajectory that serves as a path from the initial condition to the target, ψ_{targ}. This work is limited to L-mode discharges, however, if experiments were to be carried out in H-mode discharges, the feedforward optimization could be modified to include optimal timing of the L-H transition [20]. During actual physical experiments the role of the linear feedback control described in what follows is primarily to eliminate deviations from the desired trajectory due to perturbations in the initial condition, disturbances, and unmodeled dynamics.

B. Model Order Reduction and Linearization

To facilitate control design, the model is reduced to a finite set of ordinary differential equations (ODEs) by using finite difference approximations to the spatial derivatives. The non-dimensional domain of interest, $\hat{\rho} = [0, 1]$, is represented as l nodes, and the spacing between the nodes is defined as $\Delta\hat{\rho} = 1/(l-1)$. The reduced-order state space model is written as

$$\dot{\Theta} = W(\Theta, u), \quad Y = C\Theta, \tag{9}$$

where the model states are $\Theta = [\theta_2, \theta_3, \ldots, \theta_{l-1}]^T$, the model outputs are $Y = [\iota_2, \iota_3, \ldots, \iota_{l-1}]^T$, the model inputs are $u = [u_{\text{NBI},1}, \ldots u_{\text{NBI},n_{\text{NBI}}}, I_{\text{p}}]$, W is a nonlinear function, and C is given by (2). Let Θ_{FF}, Y_{FF}, and u_{FF} represent the feedforward trajectories of the states, outputs, and inputs which satisfy $\dot{\Theta}_{\text{FF}} = W(\Theta_{\text{FF}}, u_{\text{FF}})$, $y_{\text{FF}} = C\Theta_{\text{FF}}$, and let the variables $\bar{\theta} = \Theta - \Theta_{\text{FF}}$, $\bar{y} = Y - Y_{\text{FF}}$, and $u_{\text{FB}} = u - u_{\text{FF}}$ represent perturbations around the feedforward trajectory. Inserting the perturbation variables into (9) and ignoring higher order terms results in

$$\dot{\bar{\theta}} = W(\Theta_{\text{FF}}, u_{\text{FF}}) + \frac{\partial W}{\partial \Theta}(\Theta_{\text{FF}}, u_{\text{FF}})\bar{\theta} + \frac{\partial W}{\partial u}(\Theta_{\text{FF}}, u_{\text{FF}})u_{\text{FB}},$$

from which we obtain the linear dynamics around the feedforward trajectory

$$\dot{\bar{\theta}} = A_{\text{FPD}}(t)\bar{\theta} + B_{\text{FPD}}(t)u_{\text{FB}}, \quad \bar{y} = C\bar{\theta}, \tag{10}$$

where $A_{\text{FPD}} = \nabla_\Theta W|_{\Theta_{\text{FF}}, u_{\text{FF}}}$ and $B_{\text{FPD}} = \nabla_u W|_{\Theta_{\text{FF}}, u_{\text{FF}}}$. Given that we have full state measurement and the outputs have a direct one-to-one correspondence with the states, we can eliminate the output function for simplicity of control design to write, $\dot{x} = \bar{A}_{\text{FPD}}(t)x + \bar{B}_{\text{FPD}}(t)u_{\text{FB}}$, where the variable x has been introduced in place of $\bar{y}$ ($x = \bar{y}$), $\bar{A}_{\text{FPD}}(t) = CA_{\text{FPD}}(t)C^{-1}$ and $\bar{B}_{\text{FPD}}(t) = CB_{\text{FPD}}(t)$. Furthermore, assuming that the profile is controlled without transitioning to the H-mode scenario, the system can be fairly approximated by the LTI system

$$\dot{x} = Ax + Bu_{\text{FB}}, \tag{11}$$

where A and B are taken as $\bar{A}_{\text{FPD}}(t_{\text{targ}})$ and $\bar{B}_{\text{FPD}}(t_{\text{targ}})$.

C. LQI Control Design

For a requested target state, x_{t}, let x_∞^{ss} represent the closest stationary state achievable according to the model. This can be determined from the pseudo-inverse, $K_{\text{sg}}^\dagger$, of the model static gain matrix $K_{\text{sg}} = -A^{-1}B$. The input associated with the desired target is determined from the pseudo-inverse of the static gain matrix, $u_{\text{FB},\infty}^{ss} = K_{\text{sg}}^\dagger x_{\text{t}}$, which is used to determine the closest achievable stationary state given by $x_\infty^{ss} = K_{\text{sg}} u_{\text{FB},\infty}^{ss} = K_{\text{sg}} K_{\text{sg}}^\dagger x_{\text{t}}$. Because several of the actuators have similar effects on the profile, the matrix $K_{\text{sg}} = W\Sigma V^T$ is ill-conditioned, i.e. the ratio of the largest singular value to the smallest one is much larger than one. Therefore small deviations in the profile associated with the directions of the smaller singular values can result in unreasonably large control requests. Thus, we use a truncated (Tr) singular value expansion of the static gain matrix given by, $K_{\text{sg,Tr}} = W_{\text{Tr}}\Sigma_{\text{Tr}}V_{\text{Tr}}^T$, where the matrices W_{Tr}, Σ_{Tr}, and V_{Tr} are the components of the SVD associated with the n_{SV} largest singular values,

$$W = \begin{bmatrix} W_{\text{Tr}} & W_{\text{n}} \end{bmatrix}, \; \Sigma = \begin{bmatrix} \Sigma_{\text{Tr}} & 0 \\ 0 & \Sigma_{\text{n}} \end{bmatrix}, \; V = \begin{bmatrix} V_{\text{Tr}} & V_{\text{n}} \end{bmatrix}, \tag{12}$$

and W_n, Σ_n, and V_n are the components associated with the smaller, neglected singular values. Therefore,

$$u_{\text{FB},\infty}^{ss} \cong u_{\text{FB},\infty} = K_{\text{sg,Tr}}^\dagger x_t, \;\; x_\infty^{ss} \cong x_\infty = K_{\text{sg,Tr}} K_{\text{sg,Tr}}^\dagger x_t. \tag{13}$$

We use the theory of linear quadratic optimal control to obtain a control law which regulates the system to the closest achievable stationary state while minimizing the cost function

$$J = \int_0^\infty \begin{bmatrix} \tilde{x}^T(t) & \zeta^T(t) \end{bmatrix} Q \begin{bmatrix} \tilde{x}(t) \\ \zeta(t) \end{bmatrix} + \tilde{u}^T(t) R \tilde{u}(t) dt, \tag{14}$$

where $\tilde{x} = x - x_\infty$, $\tilde{u} = u_{\text{FB}} - u_{\text{FB},\infty}$, Q positive semidefinite, R positive definite, and ζ represents the integral states introduced for integral control. The added integral states are expressed as $\zeta = K_\zeta \int_0^t \tilde{x}(\tau) d\tau$, where K_ζ is a design matrix. We can note that with the choice $K_\zeta = W_{\text{Tr}}^T$, we have $K_\zeta K_{\text{sg,Tr}} K_{\text{sg,Tr}}^\dagger = K_\zeta$, since

$$\begin{bmatrix} W_{\text{Tr}}^T \end{bmatrix} \cdot \begin{bmatrix} W_{\text{Tr}} \Sigma_{\text{Tr}} V_{\text{Tr}}^T \end{bmatrix} \cdot \begin{bmatrix} V_{\text{Tr}} \Sigma_{\text{Tr}}^{-1} W_{\text{Tr}}^T \end{bmatrix} = W_{\text{Tr}}^T = K_\zeta. \tag{15}$$

This ensures $K_\zeta x_{\text{t}} = K_\zeta x_\infty$, since $x_\infty = K_{\text{sg,Tr}} u_{\text{FB},\infty} = K_{\text{sg,Tr}} K_{\text{sg,Tr}}^\dagger x_{\text{t}}$. Here, we have made use of the fact that $W_{\text{Tr}}^T W_{\text{Tr}} = I$, and $V_{\text{Tr}}^T V_{\text{Tr}} = I$, but $W_{\text{Tr}} W_{\text{Tr}}^T \neq I$.

Written in terms of the requested target ($\tilde{x}(t) = x(t) - K_{\text{sg,Tr}} K_{\text{sg,Tr}}^\dagger x_t(t)$), the control law that minimizes (14) reduces to a proportional plus integral controller of the form

$$\begin{aligned} u_{\text{FB}}(t) = u_{\text{FB},\infty} &- K_{\text{p}} \left[x(t) - K_{\text{sg,Tr}} K_{\text{sg,Tr}}^\dagger x_t(t) \right] \\ &- K_{\text{i}} K_\zeta \int_0^t \text{d}\tau \left[x(\tau) - K_{\text{sg,Tr}} K_{\text{sg,Tr}}^\dagger x_t(\tau) \right], \end{aligned} \tag{16}$$

where the proportional gain, K_{p}, and integral gain, K_{i}, are given by $\begin{bmatrix} K_{\text{p}} & K_{\text{i}} \end{bmatrix} = R^{-1}\hat{B}S$, where $S = S^T$ is the unique positive semi-definite solution to the algebraic Ricatti equation, $\hat{A}^T S + S\hat{A} - S\hat{B}R^{-1}\hat{B}^T S + Q = 0$, and the system

$(\hat{A}, \hat{B})$ is constructed by augmenting the model (11) with the integrator states, i.e.

$$\begin{bmatrix}\dot{\tilde{x}}\\ \dot{\zeta}\end{bmatrix} = \underbrace{\begin{bmatrix}A & 0\\ K_\zeta & 0\end{bmatrix}}_{\hat{A}}\begin{bmatrix}\tilde{x}\\ \zeta\end{bmatrix} + \underbrace{\begin{bmatrix}B\\ 0\end{bmatrix}}_{\hat{B}}\tilde{u}. \tag{17}$$

The design parameters include $K_\zeta = W_{\text{Tr}}^T$, Q and R. The state weighting matrix, Q, is chosen as $Q = \begin{bmatrix}\hat{Q} & 0\\ 0 & \alpha_\zeta^2 I_{n_{\text{SV}}}\end{bmatrix}$, where α_ζ is a constant that weights the integrator states relative to the model states, $\hat{Q}$ is the weighting on the model states and R is chosen diagonal.

D. Two Loop LQI Controller

Via a two loop feedback controller, the total plasma current is used to regulate the profile at the plasma edge and the NBI are used to regulate the interior profile. This approach of focusing the total plasma current on edge regulation and NBI on interior regulation is well conceived when combined with optimized feedforward control, which provides not only a feedforward control action but also an optimal trajectory (path) to the target profile. The feedback controller simply has to follow the desired trajectory produced by the optimized trajectory design. To construct the two-loop controller, the inputs of the LTI system (11) are separated into the NBI powers, $\tilde{u}_{\text{NBI}}$, and the total plasma current, $\tilde{u}_{I_\text{p}}$,

$$\dot{\tilde{x}} = A\tilde{x} + \begin{bmatrix}B_{\text{NBI}} & B_{I_\text{p}}\end{bmatrix}\begin{bmatrix}\tilde{u}_{\text{NBI}}\\ \tilde{u}_{I_\text{p}}\end{bmatrix}. \tag{18}$$

For the inner loop controller, we consider only the response of the edge value, to the total plasma current,

$$\begin{aligned}\dot{\tilde{x}} =& A\tilde{x} + B_{I_\text{p}}\tilde{u}_{I_\text{p}},\\ \tilde{x}_B =& C_{I_\text{p}}\tilde{x},\end{aligned} \tag{19}$$

where $C_{I_\text{p}} = [0, 0, ..., 1]$, and $\tilde{x}_\text{B}$ is the value of $\tilde{x}$ at the edge. The controller is constructed by first augmenting the system (19) with the integrator state, $x_c = C_{I_\text{p}}\int \tilde{x}dt$,

$$\begin{bmatrix}\dot{\tilde{x}}\\ \dot{x}_c\end{bmatrix} = \begin{bmatrix}A & 0\\ C_{I_\text{p}} & 0\end{bmatrix}\begin{bmatrix}\tilde{x}\\ x_c\end{bmatrix} + \begin{bmatrix}B_{I_\text{p}}\\ 0\end{bmatrix}\tilde{u}_{I_\text{p}}, \tag{20}$$

and then by solving for the linear control policy, $\tilde{u}_{I_p} = -K_{\text{LQI}}[\tilde{x}^T\ x_c^T]^T$, following the approach explained in Section III-C. The gain matrix can be partitioned into $K_{\text{LQI}} = [K_{\text{P},\tilde{x}}\ K_{\text{I},x_c}]$, where $K_{\text{P},\tilde{x}}$ are gains on the $\tilde{x}$ and K_{I,x_c} is the gain on the integrator state x_c. For a state space description of the controller, we have

$$\begin{aligned}\dot{x}_c =& 0x_c + C_{I_\text{p}}\tilde{x},\\ \tilde{u}_{I_\text{p}} =& -K_{\text{P},\tilde{x}}\tilde{x} - K_{\text{I},x_c}x_c.\end{aligned} \tag{21}$$

Combining (21) with the plant (18), we close the inner loop to obtain,

$$\begin{bmatrix}\dot{\tilde{x}}\\ \dot{x_c}\end{bmatrix} = \begin{bmatrix}A - B_{I_\text{p}}K_{\text{P},\tilde{x}} & -B_{I_\text{p}}K_{\text{I},x_c}\\ C_{I_p} & 0\end{bmatrix}\begin{bmatrix}\tilde{x}\\ x_c\end{bmatrix} + \begin{bmatrix}B_{\text{NBI}}\\ 0\end{bmatrix}\tilde{u}_{\text{NBI}}. \tag{22}$$

For the outer loop controller, again we proceed with LQI design, but now applied to the system (22). In this case, the inputs, which are solely the NBI, are used to control the interior profile shape. First, the system (22) is augmented with the integrator states, $\zeta = \hat{K}_\zeta\int \tilde{x}dt$. Then, the open loop system augmented with integrator states can be written as

$$\begin{bmatrix}\dot{\tilde{x}}\\ \dot{x}_c\\ \dot{\zeta}\end{bmatrix}\begin{bmatrix}A - B_{I_\text{p}}K_{\text{P},\tilde{x}} & -B_{I_\text{p}}K_{\text{I},x_c} & 0\\ C_{I_p} & 0 & 0\\ \hat{K}_\zeta & 0 & 0\end{bmatrix}\begin{bmatrix}\tilde{x}\\ x_c\\ \zeta\end{bmatrix} + \begin{bmatrix}B_{\text{NBI}}\\ 0\\ 0\end{bmatrix}\tilde{u}_{\text{NBI}}, \tag{23}$$

for which, the LQI gains are given by $\hat{K}_{LQI} = \begin{bmatrix}\hat{K}_{\text{P}\tilde{x}} & \hat{K}_{\text{P},x_c} & \hat{K}_{\text{I},\zeta}\end{bmatrix}$. Then the outer loop controller can be written as

$$\begin{aligned}\dot{\zeta} =& 0\zeta + \hat{K}_\zeta\tilde{x},\\ \tilde{u}_{\text{NBI}} =& -\hat{K}_{\text{P},\tilde{x}}\tilde{x} - \hat{K}_{\text{P},x_c}x_c - \hat{K}_{\text{I},\zeta}\zeta,\end{aligned} \tag{24}$$

which can be combined with the inner loop controller (21). The final feedback controller can be written in terms of the measurement x and the target x_t ($\tilde{x} = x - K_{\text{sg,Tr}}K_{\text{sg,Tr}}^\dagger x_t$) as

$$\begin{aligned}\begin{bmatrix}\dot{\zeta}\\ \dot{x_c}\end{bmatrix} &= \begin{bmatrix}0 & 0\\ 0 & 0\end{bmatrix}\begin{bmatrix}\zeta\\ x_c\end{bmatrix} + \begin{bmatrix}\hat{K}_\zeta\\ C_{I_\text{p}}\end{bmatrix}\tilde{x},\\ \begin{bmatrix}\tilde{u}_{\text{NBI}}\\ \tilde{u}_{I_\text{p}}\end{bmatrix} &= \begin{bmatrix}-\hat{K}_{I,\zeta} & -\hat{K}_{P,x_c}\\ 0 & -K_{I,x_c}\end{bmatrix}\begin{bmatrix}\zeta\\ x_c\end{bmatrix} + \begin{bmatrix}-\hat{K}_{\text{P},\tilde{x}}\\ -K_{\text{P},\tilde{x}}\end{bmatrix}\tilde{x}.\end{aligned} \tag{25}$$

A SVD analysis of the linearized system's response to the NBI is shown in Fig. 2. The analysis shows the directions in which the profile can be significantly manipulated by the NBI in steady state. The columns of input singular matrix, Fig. 2(a), represent linear combinations of the NBI powers and the output singular vectors scaled by the singular values, $U\Sigma$, represent the response to those input combinations, Fig. 2(c). Only the first three directions are plotted since the remaining singular values are very small. Based on the output directions shown in Fig. 2(c), the NBI can only significantly influence the profile in two directions. Therefore two singular values are used in the truncated singular value decomposition.

IV. Experimental Setup and Results

A. Goal of the Experiment

In all cases, the goal is to obtain a certain target q profile at a certain time while maintaining the plasma in the L-mode regime. We test three targets, each with increasing difficulty to achieve. The targets are all monotonically increasing q profiles with varying levels of q at the plasma center and plasma edge. It is desirable to obtain a large total plasma current while also maintaining q high at the center, i.e. a current profile that is low at the center or not too peaked. Our primary goal is to obtain reproducibility between experiments by reliably obtaining the desired target in the startup phase or coming as close as possible. If and when the target is obtained, control of the remainder of the discharge would be assumed by some other experiment. Therefore we are not concerned with reaching the target in a steady state.

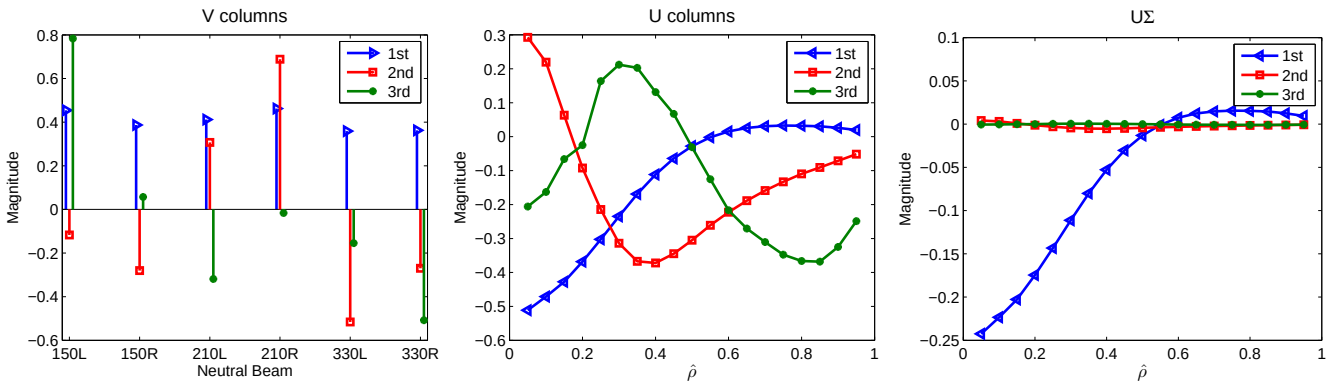

(a) V columns. (b) U columns. (c) $U\Sigma$ columns.

Fig. 2. SVD analysis of the linearized model including only the effects of the NBI. (a.) Input singular vectors, i.e. columns of V, which represent combinations of the NBI powers. (b.) Output singular vectors, i.e. columns of U, which represent deviations from the nominal profile associated with the input combinations. (c.) Output singular vectors scaled by the singular values.

B. L-H Transition Power Limit

To avoid L-H transitions, a total auxiliary power limit was imposed during the experiments. For each experiment the imposed power limit is marked by green x, see Fig. 4(a)-Fig. 4(c). First, we experimented with simple fixed power limits. For example in Fig. 4(a), the NBI auxiliary power was limited to 5 MW. During testing of Target 1, the H-mode transition power was observed to approximately scale with the electron density according to

$$P_{\text{LH}} = 2\bar{n}_e^{3/2}. \tag{26}$$

During subsequent experiments, testing of Target 2 and 3, the total injected power was constrained by this limit, Fig. 4(b) and 4(c). The limit (26) was also used as a constraint in the feedforward optimization as discussed in Section III-A.

C. Summary of Experimental Results

The obtained q profile for each of the three targets are shown in Fig. 3 and the corresponding total injected auxiliary power is shown in Fig. 4. In Fig. 3, we show both the obtained q profile with feedforward (FF) control alone and combined feedforward and feedback (FF+FB) control at the best-matching time. In all cases, feedback control improves the obtained q-profile matching error by about 50%, even with wildly different initial conditions.

The q profile is physically limited to a value greater than one; if it falls to one, an undesirable phenomenon known as saw-teeth will prevent it from falling further, essentially resetting it above one. Usually, the q profile with FF control alone falls to one before the target time regardless of the initial condition. This result is primarily due to slight modeling errors in the current diffusion rate, which lead to a nonsatisfactory feedforward control policy calculated by the trajectory optimization of Section III-A. This emphasizes the importance of feedback control, which is able to account for the modeling errors and bring the q profile back on target or at least as close as possible. See Figure 5 for a comparison of q at the center with FF control alone and FF+FB control. The controller successfully obtains Target 1 (Fig. 5(a)), and comes very close to obtaining Targets 2 (Fig 5(b)) and 3 (Fig. 5(c)). However, for both target 2 and 3 cases, the NBI power is almost always at the H-mode transition limit. Further experiments tested with a different type of controller showed that it was indeed possible to achieve Target 2 and Target 3 by relaxing the L-H transition power limit.

V. Summary and Conclusions

We considered a first-principles-driven, control-oriented dynamic model describing the evolution of the poloidal flux profile and therefore the current profile during L-mode tokamak discharges. Combining feedforward optimization via nonlinear programming and active feedback control via LQI we were able to realize reliable attainment of certain q profiles in the L-mode phase of the tokamak discharge.

References

[1] E. Strait and the DIII-D Team, "DIII-D research in support of ITER," *Nucl. Fusion*, vol. 49, no. 104008, 2009.

[2] M. Murakami *et al.*, "Progress towards fully noninductive, high beta conditions in DIII-D," *Physics of Plasmas*, vol. 13, p. 056106, 2006.

[3] A. G. Peters, "The bootstrap current and its consequences," *Plasma Phys. and Control. Fusion*, vol. 42, p. B231, 2000.

[4] T. Luce and the DIII-D Team, "Development of burning plasma and advanced scenarios in the DIII-D tokamak," *Nuclear Fusion*, vol. 45, p. S86, 2005.

[5] S. Ide and the JT-60 Team, "Overview of JT-60U progress towards steady-state advanced tokamak," *Nuclear Fusion*, vol. 45, p. S48, 2005.

[6] Y. Ou, T. Luce, E. Schuster *et al.*, "Towards model-based current profile control at DIII-D," *Fusion Engineering and Design*, vol. 82, pp. 1153–1160, 2007.

[7] E. Witrant *et al.*, "A control-oriented model of the current profile in tokamak plasmas," *Plasma Phys. and Control. Fusion*, vol. 49, pp. 1075–1105, 2007.

[8] F. Felici *et al.*, "Real-time physics-model-based simulation of the current density profile in tokamak plasmas," *Nuclear Fusion*, vol. 51, no. 083052, 2011.

[9] J. Barton, W. Shi *et al.*, "Physics-based Control-oriented Modeling of the Current Density Profile Dynamics in High-performance Tokamak Plasmas," *52nd IEEE International Conference on Decision and Control*, 2013.

[10] F. Hinton and R. Hazeltine, "Theory of plasma transport in toroidal confinement systems," *Rev. Mod. Phys.*, vol. 48, pp. 239–308, 1976.

[11] J. Barton, M. Boyer, W. Shi, E. Schuster *et al.*, "Toroidal Current Profile Control During Low Confinement Mode Plasma Discharges in DIII-D via First-Principles-Driven Model-based Robust Control Synthesis," *Nuclear Fusion*, vol. 52, no. 123018, 2012.

[12] S. Kim and J. Lister, "A potentially robust plasma profile control approach for ITER using real-time estimation of linearized profile response models," *Nuclear Fusion*, vol. 52, p. 074002, 2012.

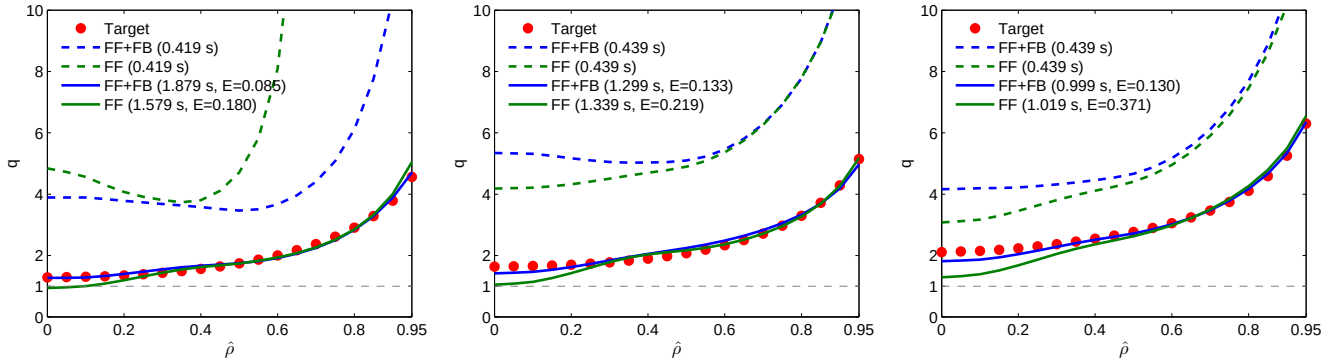

(a) Shot 156806 Target 1 (b) Shot 157954 Target 2 (c) Shot 158056 Target 3

Fig. 3. Obtained q profiles for each of the three targets with FF control and FF+FB control at the time associated with the best profile matching. The red circles mark the target q profiles, the dash lines mark the initial conditions and the solid lines mark the obtained q profiles. In each case, FF-control-only shots are in green and FF+FB control shots are in blue. Generally, the initial conditions vary significantly from shot to shot.

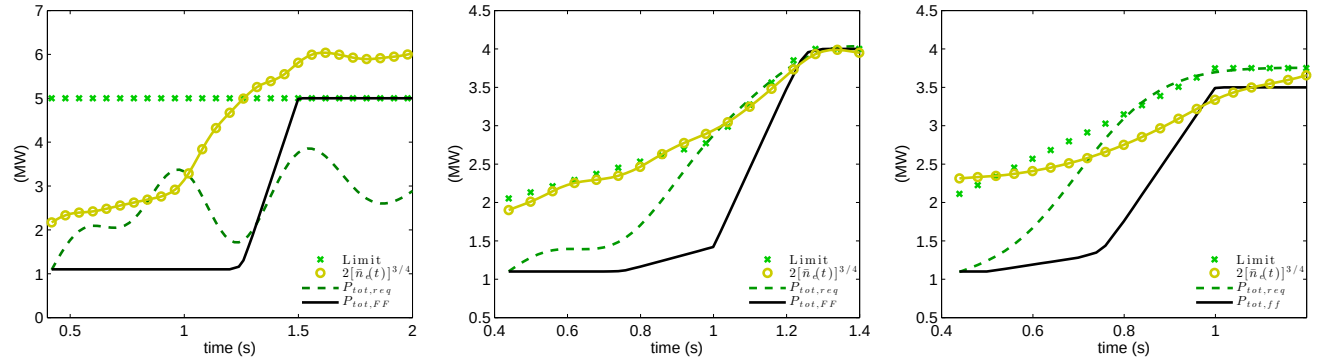

(a) Shot 156806 Target 1 (b) Shot 157954 Target 2 (c) Shot 158056 Target 3

Fig. 4. Total auxiliary power during the experiment. The predicted L-H power transition threshold, P_{LH} is marked with gold circles and the imposed power limit is marked with green stars. FF NBI power is shown in solid black, while FF+FB NBI power is shown in dashed green.

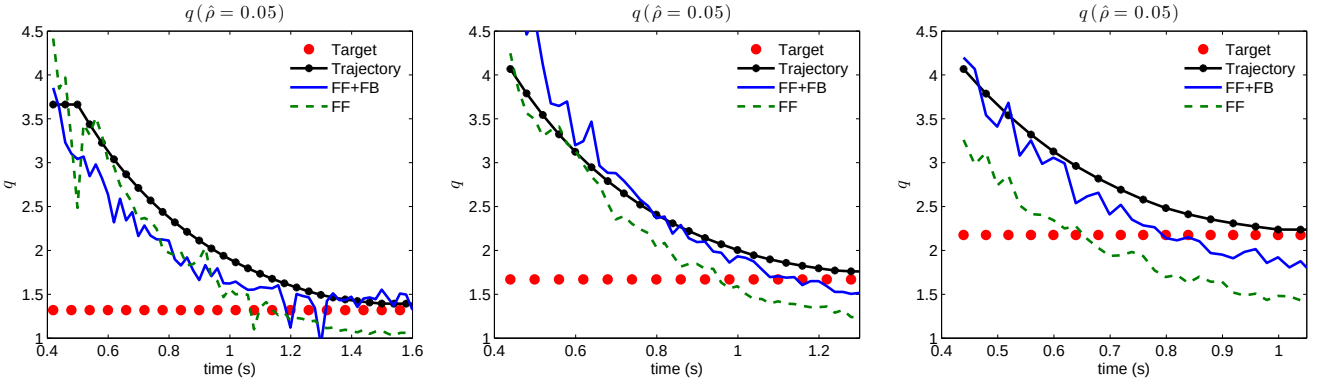

(a) Shot 156806 Target 1 (b) Shot 157954 Target 2 (c) Shot 158056 Target 3

Fig. 5. Center q profile value obtained during FF and FF+FB control experiments for each target. The black line ("Trajectory") represents the time evolution of the target profile at $\hat{\rho} = 0.05$ used by the feedback controller. As it can be noted from the figure, the black line matches the red line ("Target") at the desired matching time (1.6s for Target 1, 1.3s for Target 2, 1.0s for Target3).

[13] F. Arogmendo *et al.*, "Lyapunov-based Distributed Control of the Safety-factor Profile in a Tokamak Plasma," *Nuclear Fusion*, vol. 53, no. 3, p. 033005, 2013.

[14] M. Boyer, J. Barton, E. Schuster *et al.*, "Backstepping Control of the Toroidal Plasma Current Profile in the DIII-D Tokamak," *IEEE Transactions on Control Systems Technology*, vol. 22, no. 5, pp. 1725–1739, 2014.

[15] J. Wesson, *Tokamaks*. Oxford, UK: Clarendon Press, 1984.

[16] O. Sauter *et al.*, "Neoclassical conductivity and bootstrap current formulas for general axisymmetric equilibria and arbitrary collisionality regime," *Physics of Plasmas*, vol. 6, no. 7, p. 2834, 1999.

[17] ——, "Erratum: Neoclassical conductivity and bootstrap current formulas for general axisymmetric equilibria and arbitrary collisionality regime [Phys. Plasmas 6, 2834 (1999)]," *Physics of Plasmas*, vol. 9, no. 12, p. 5140, 2002.

[18] M. Boyer, J. Barton, E. Schuster *et al.*, "First-Principles-Driven Model-Based Current Profile Control for the DIII-D Tokamak via LQI Optimal Control," *Plasma Physics and Controlled Fusion*, vol. 55, no. 105007, 2013.

[19] J. Barton, E. Schuster *et al.*, "Nonlinear Physics-model-based Actuator Trajectory Optimization for Advanced Scenario Planning in the DIII-D Tokamak," in *19th IFAC World Congress*, 2014, pp. 671–676.

[20] J. van Dongen, F. Felici, G. M. D. Hogeweij, P. Geelen, and E. Maljaars, "Numerical optimization of actuator trajectories for ITER hybrid scenario profile evolution," *Plasma Physics and Controlled Fusion*, vol. 56, no. 12, p. 125008, 2014.